Egypt. J. Chem. **Vol. 65,** No. SI:13, pp. 53 – 70 (2022)

Egyptian Journal of Chemistry

http://ejchem.journals.ekb.eg/

Modified Cellulose Acetate Membrane for Industrial Water Purification

Amina L. Mohamed * and Ahmed G. Hassabo

National Research Centre (Scopus affiliation ID 60014618), Textile Research and Technology Institute, Pre-treatment, and Finishing of Cellulose-based Textiles Department, 33 El-Behouth St. (former El-Tahrir str.), Dokki, P.O. 12622, Giza, Egypt

Abstract

The water industry needs to develop economical and stable materials and methods for providing adequate quantities of fresh water. Cellulose acetate material is widely used in many important applications. The motivation lies not only in the economic and ecological advantages of using cellulose-based materials but also in the advantageous characteristics and properties of these materials. This project aims to provide a better understanding of process-structure-property relationships with advanced functionalities in a new modification of cellulose acetate and to show potential large-scale processability. An important expected result for composite-based cellulose acetate materials is the favorable combination of excellent mechanical properties. The possible applications of the modified cellulose acetate membrane for removing various contaminations from polluted waters will be investigated. To achieve this goal, the main tasks of the research project this year are the synthesis and modification of cellulose acetate and in situ preparation of some nanoparticles and their characterization. In this concept, cellulose acetate was synthesized via acetylation of cotton west and characterized using XRD and FT-IR. The prepared cellulose derivative was subjected to chemical modification to create silicones moieties in its structure, then the new composite was used for in situ preparation of some nanoparticles. The nanoparticles (silver, zinc, zirconium, titanium, and silica) were successfully prepared and characterized using TEM, SEM, and XRD. The next step of the project will be the production of membranes and ex situ preparation of nanoparticles then mixed with the modified cellulose acetate and the production of another type of membrane..

Keyword: Cellulosic-based materials, membranes, composite, metal nanoparticles, water treatment

1. Introduction

The world's single largest water problem is its scarcity. Water is an indispensable commodity for the sustenance of all living organisms. It is utilized for many functions, which include domestic, agricultural, and industrial applications. Industrial wastewater often contains higher metals along with other anions and treatment is necessitated in parliamentary procedure to avoid water contamination. Heavy metal contamination of varied water resources is of immense concern considering the toxic effect on human beings and other living organisms in the environment. There are one billion people who do not have access to a reliable source of safe drinking water and according to this situation, around 6000 children die daily due to dehydration caused by various pathogens in polluted water. **[1, 2]**

Membranes can produce high-quality drinking water from fresh, brackish, seawater, and water reuse sources. Common membrane processes include microfiltration (MF), ultrafiltration (UF), nanofiltration (NF), and reverse osmosis (RO). Membranes are made from many types of polymers, such as polyacrylonitrile (PAN), polyamide (PA), polyimide (PI), poly(tetrafluoroethylene) (PTFE), poly(vinylidene fluoride) (PVDF), polysulfone (PSF), polyethersulfone (PES), cellulosic, etc. **[3-5]** Cellulose can be processed at relatively low cost and has interesting properties including a low density, a high tensile strength, and a high Young's modulus which make this material very attractive for several

*Corresponding author e-mail: alo.mohamed12@hotmail.com, Tel.: +20 110 22 555 14

Receive Date: 27 June 2022, **Revise Date:** 13 July 2022, **Accept Date:** 15 August 2022, **First Publish Date:** 15 August 2022
DOI: 10.21608/EJCHEM.2022.147513.6393

applications like as a fibrous material in paper and filters, in composite materials, and as pulp. **[6-10]**

Nanoparticle-doped Mixed Matrix Membrane (MMMs) is gaining considerable interest amongst researchers today. MMMs can be made to specifically remove targeted contaminants and they improve mechanical, thermal, magnetic, and electrostatic properties and intensify solute, diffusivity, selectivity, anti-bacterial property, and lower flux decline. **[11-13]** Generally, nanocomposite membranes are prepared by introducing nanoparticle materials (the filler) into a macroscopic sample material (the matrix). Nanoparticles may be either coated onto the membrane surface or dispersed in the polymer solution before membrane casting. [14-44]

In this framework, secondary materials commonly known as fillers are incorporated into the main polymeric matrix to generate polymer-nanocomposite membranes, which are also referred to as mixed matrix membranes or nano-enhanced membranes. The nanocomposite membranes are a potential alternative to face all these challenges. The fabrication and use of these membranes are one of the current applications of nanotechnology in membranes for water treatment. For example, nanoparticles-based membranes have demonstrated a low-fouling process by adding inorganic particles. Dispersing the nanoparticles (NPs) into the polymer generally forms these composite membranes, which are also a suitable tool to improve the performance, such as permeability and selectivity, in polymeric membranes. Typically, the addition of the fillers tends to change the surface properties of membranes influencing the separation performance, e.g., high permeability, stable flux, excellent rejection against foulants, and better antifouling behavior. **[11, 45-51]**

In the present work, cellulose-based membrane and filters with adsorbed metal nanoparticles will be obtained. In this way, cellulose acetate will be modified and grafted or coated with functional polymers. The nanoparticles will be formed and adsorbed at the external surface of the membranes causing a change in the chemical composition of this surface layer providing also possible surface properties alterations. The obtained membranes will be characterized by scanning electron microscopy, X-ray diffraction, and measurements of thickness, porosity, specific surface area, pore diameter and volume, water contact angle, and permeability. Nanoparticles released from these membranes will be also measured.

2. Experimental

2.1. Materials

The cotton waste was obtained from a local area in Egypt. The collected cotton was washed and dried at 70°C for 24 h. Before the hydrolysis process, the cotton was bleached. All chemicals were analytical grade and were used as received.

Aminopropyl isobutyl POSS, toluene-2,4-diisocyanate (TDI), dibutyltindilaurate, 1-methyl-2-(pyrrolidinone)(NMP) were purchased from Fluka. Silver nitrate, zinc acetate, zirconium isopropoxide ($Zr(C_3H_7O)_4$), sodium silicate, titanium (IV) isopropoxide $Ti(OC_3H_7)_4$, sulfuric acid, Acetic acid, sodium carbonate, sodium hydroxide, hydrochloric acid, toluene, ethanol (CH_2CH_3OH, 99.9%), sodium lauryl sulfate were purchased in analytical grade.

2.2. Methods

2.2.1. Hydrolysis of cotton

Cotton hydrolysis was done with sulfuric acid concentrations (30 % v/v). It was carried out in a 500 ml Erlenmeyer flask containing one gram of cotton waste and a solution of sulphuric acid. The mixture was constantly mixed for 90 min at 250 rpm. The mixture was mixed with cold distilled water (to stop the hydrolysis process). The leftovers were rinsed with distilled water repeatedly and attained a neutral pH (pH of 6-7). They were then dried for 24 hours at 50°C.

2.2.2. Acetylation of cellulose obtained from cotton

Acetic acid was used to add two grams of cellulose to Erlenmeyer's flask with 70 mL of distilled water and then stirred to create a slurry. Added to slurry NaOH (1 M, 1 mL) (pH 8). The mixture was mixed with acetic acid (4.8 mL) and constantly stirred for 1 hour at 40°C. The pH was thereafter adjusted to room temperature for the original pH (pH 8). The reaction was halted after 30 minutes (acetylation reaction) by the addition of HCl (pH 5.5). Finally, the cellulose was rinsed with distilled water repeatedly until a neutral pH was obtained and then dried at 50°C [3].

2.2.3. Modification of cellulose acetate with Aminopropyl POSS

In the first step, aminopropyl isobutyl POSS (1g,1.434 mmol), toluene-2,4-diisocyanate (TDI, 0.1999 g,1.434 mmol), and toluene (20 mL) were placed in a 100 mL two-necked round bottom flask equipped with a magnetic stirrer, reflux condenser, and N_2 purge. The temperature of the stirred reaction mixture solution was raised to 80°C, and after approximately 15 min, a catalytic amount of dibutyltin dilaurate (0.1mL) was added to the mixture. The reaction progress was monitored by FT-IR spectroscopy, as the disappearance of the $–NH_2$ peak indicated completion of the preferential reaction

between the para-isocyanate of the TDI compound and the amine group of the aminopropyl isobutyl POSS to give POSS–TDI. In the next step, cellulose acetate (13.27 g) which had been dried overnight at 110°C was dissolved in 1-methyl-2-(pyrrolidinone)(NMP) and then added to 6 mL (0.442 mmol) of the POSS–TDI solution. The reaction mixture was heated to 50°C and the reaction progress was monitored by FT-IR spectroscopy, as the disappearance of the isocyanate peak indicated that the reaction had gone to completion. The CA–POSS additive was vacuum-dried at 40°C for24h, and then the CA–POSS was used in the membrane casting.

2.2.4. In-situ Preparation of different nano-metal and/or metal oxide in Cellulose Acetate/ polymer composite

2.2.4.1. Synthesis of silver nanoparticle

Silver nitrate solution (1 mol/L) was added to an aqueous of modified cellulose acetate (5 w/v %, 200 ml) until a final concentration of 1 mmol/L and then incubated at 80°C, 200 rpm for 30 min, in the absence of light. The synthesis of silver nanoparticles was confirmed by the color change of the solution and the presence of a plasmonic band in 420 nm. Ultraviolet-visible (UV-Vis) spectral analysis was done by using Cary 100 Agilent Spectrophotometer in the range of 200 to 800 nm.

2.2.4.2. Synthesis of Zinc oxide nanoparticle

Zinc oxide nanoparticles (ZnONPs) have been synthesized using the modified method from the reported one by Rajendra et al [52] from zinc acetate as precursors and reduced in the presence of modified cellulose acetate as a capping agent by use of sodium carbonate to adjust the pH medium to 10.

In this modified procedure, 70 ml of 2% cellulose acetate (as a capping agent) was placed in a beaker and the pH medium was adjusted to 10 using sodium carbonate (10%). After that, the solution temperature was raised to 70°C, and 1 N zinc acetate in 30 ml distilled water was added to the solution of modified cellulose acetate drop by drop under stirring for 30 minutes. Then the solution was kept at this temperature for 90 min. under stirring. The produced powder was filtered and dried at 90°C for 24 h. the produced powder was combinations of $Zn(OH)_2$, and $Zn(CO_3)_2$ or combinations between them as $Zn_5(OH)_6(CO_3)_2$. **[24]** So, the calcination step is important to form ZnONPs at it was done at 400°C for 4 hr. The calcinated ZnONPs were used for further use.

2.2.4.3. Synthesis of Zirconium oxide nanoparticle

The sol-gel method was used to synthesize the solids based on zirconia, under a nitrogen atmosphere. The zirconium isopropoxide (1.2 moles, $Zr(C_3H_7O)_4$), was used as precursor zirconia. acetic acid (99.99%) was used as a catalyst whereas absolute ethanol (CH_2CH_3OH, 99.9%) (EtOH), and distilled water was used as solvents in all the synthesis.

Wherein modified cellulose acetate (2 g) was placed in a beaker, 80 ml ethanol/water (80:20) and the 2 ml acetic acid catalyst were placed, the precursor was then incorporated and, preceded to the addition of the remaining amount of solvent (up to 100 ml) followed by the addition of 2 mmol of sodium lauryl sulfate with constant stirring. Subsequently, continuous stirring was performed for 2 h. Finally, wet gel particles were dried at room temperature and atmospheric pressure until complete solidification.

The produced powder was a combination of $ZrO(OH)_2$, and $ZrO(CO_3)$. So, the calcination step is important to forming ZrO_2NPs it was done at 600°C for 5 hr. The calcinated ZrO_2NPs were used for further use.

2.2.4.4. Synthesis of Silica nanoparticle

Modified cellulose acetate and sodium silicate are used in the preparation of Silica (SiO_2) nanoparticles. Typically, 10 g of sodium silicate was dissolved in 80 ml modified cellulose acetate solution (2%). After the temperature was raised to 60°C under gentle stirring, 20 ml of HCl (3.5% w/v) was added drop-wise to the solution. The mixture was kept under stirring until a cloudy, viscous gel is formed. The silica prepared was then thoroughly washed with distilled water until free from Cl^- ions and collected by using a centrifuge followed by drying at 60°C in the air-drying oven. Eventually, the dried sample was calcinated at 800°C for 3 hours.

2.2.4.5. Synthesis of titanium dioxide nanoparticle

6 ml of titanium (IV) isopropoxide $Ti(OC_3H_7)_4$ was added drop-wise in isopropyl alcohol and stirred. Modified cellulose acetate solution (2%) was added to the reaction medium to obtain a net volume of 50 mL and then, stirred for 30 min. The oxide gel was produced by increasing the pH by drop-wise addition of 3 ml of ammonia solution. The resultant solution was stirred for 24 h and kept for 1-day of aging. The solution was filtered after 1 day of aging to remove any particulates. The precipitate was washed several times with distilled water and dried in an oven for 24 h to remove the solvent. Removal of residual organics and the stabilization of the materials were

carried out by calcination for 3 h at 600°C. The dried powder was kept for further characterization.

2.2.5. Membrane casting

Solutions were made by slowly adding modified cellulose acetate or cellulose acetate (25 wt%) to acetone (45 wt%, 11.5 mL) and formamide (30 wt%, 5.3 mL) with stirring [19]. If a nanofiller additive was used (POSS or CA–POSS), it was dissolved in the acetone before the addition of cellulose acetate and formamide. Due to the low solubility, the solutions were left covered in the fridge overnight to allow complete dissolution. Cellulose membranes (with and without nanofiller additive) were prepared by casting them onto a glass plate. Then drawn out into a film using a casting blade set at a thickness of 0.25 mm. The membrane was allowed to air-dry for the 90s before the entire plate was immersed in an ice/water bath for 90 min. It was then immersed in a water bath at 90°C for10 min. The membrane was stored in water until used, or, if the membrane was being dried for characterization, water was exchanged with iso-propanol, then n-hexane before drying.

2.3. Characterization

The synthesized materials were investigated and monitored using a scanning electron microscope - JSM 5400 instrument (Joal, Japan). The particle shape and size were investigated and monitored using Transmission Electron Microscopy (JEOL, JEM 1200). Fourier Transform Infrared (FT-IR) spectra for synthesized materials were measured using a JASCO spectrometer with an Attenuated Total Reflectance (ATR) diamond crystal. The X-ray diffraction (XRD) experiment was conducted on a Rigaku D/MAX-IIIV X-ray Diffractometer using Ni-filtered Cu-Ka radiation with a scanning rate of 4/min at 30 kV and 20 mA.

2.4. Determination of Surface Area and Pore Diameter

Brunauer–Emmett–Teller (BET) theory was used to explain the membrane surface area, pore size diameter, and the physical adsorption of gas molecules on a solid surface [44]. The nitrogen adsorption-desorption isotherm data using Bel Sorb Max device (Japan) can be expressed as follows:

$$v = \frac{v_m c p}{(p_o - p)[1 + (c-1)(\frac{p}{p_o})]}$$

where v is the adsorbed gas volume, v_m is the adsorbed monolayer volume, p is the equilibrium gas pressure, p_o is the saturation pressure and c is the BET constant. The rearrangement of the above equation to a linear form can be expressed as follows:

$$\frac{1}{v[(\frac{p}{p_o}) - 1]} = \frac{c-1}{v_m c}\left(\frac{p}{p_o}\right) + \frac{1}{v_m c}$$

Plotting of the previous equation between $\left(\frac{p}{p_o}\right)$ and $\frac{1}{v[(\frac{p}{p_o})-1]}$. The intercept and slope function can be used to determine the constants $c = \frac{slope}{intercept} + 1$ and $v_m = \frac{1}{slope+intercept}$. The specific surface area (S, surface area per unit mass) can be calculated by the equation:

$$S = \frac{v_m N A}{22400 \times m}$$

where N is Avogadro's number, A is the cross-sectional surface area of a single adsorbed gas molecule; m is the mass of nanomaterials used in the measurement, and Standard Temperature and Pressure (STP) represents as 22400. The standard temperature used is 273 Kelvin or 0°C, and the standard pressure is 1 atmosphere (760 mm Hg). At STP, one mole of any gas occupies a volume of 22.4 litres (22400 ml). The surface area (area/mass; m^2/g) can be converted to a volume-specific surface area via multiplying by the material density.

According to Wheeler's equation, a change in pore volume or surface area can offset the pore diameter.

$$d(nm) = \frac{4000 \times V(ml/g)}{S(m^2/g)}$$

where d is the mean pore diameter, V is the total pore volume, and S is the surface area.

2.5. Water treatment

The removal of pollutants (Reactive Black 5 (RB5) as an example) from wastewater using prepared membranes or filters as adsorbents will be studied and evaluation will be done through kinetic and isothermal studies. Absorbing of dye (as a pollutants example) using prepared membranes was monitored and investigated.

2.5.1. Color removal studies

The batch systems were performed by dissolving a constant concentration of RB5 (100 mg/l) in distilled water using Erlenmeyer flasks and various amounts of the prepared membrane (0.5 -20 g). The color removal efficiency of the RB5 was measured using a UV/visible-spectrophotometer at λ_{max}= 597 nm and determined according to the following equation [23,45]:

RB5 removal efficiency (%) = $\frac{A_0 - A_1}{A_0} \times 100$

where A_0 and A_1 are the dyebath absorbances before and after dye adsorption, respectively.

2.5.2. Adsorption and isothermal studies

Adsorption isotherms experiments were performed for the modified cellulose acetate membrane with and without metal nanoparticles (in-situ and ex-situ) [4,52]. Varying quantities of the membrane (0.5-20 g/l) were applied to Erlenmeyer flasks containing 100 ml of an RB5 solution 25–300 mg/l.

The flasks were well shaken for 3 h at room temperature until equilibrium was reached. Upon separation of the membrane, a UV / visible spectrophotometer was used to measure the concentration of the RB5 in the solution at 597 nm.

For kinetic tests, sampling was performed at different time intervals (10–240 min) after the procedure, 5 ml of the residual RB5 concentration was measured using a UV – Vis spectrophotometer, and the amount of RB5 adsorbed by the membrane was determined in triplicate experiments to check the results.

The results were analyzed in three separate kinetic models: i) pseudo-first-order, ii) pseudo-second-order model, and Cegarra – Puente equation [4,53,54].

The formula of the pseudo-first-order value is shown below:

$\frac{dq}{dt} = k_1(q_e - q_t)^n$ ➔ $\ln(q_e - q_t) = \ln(q_e) - k_{e1}t$ for n=1(first-order reaction)

where q_t is the amount of dye adsorbed (mg/g) at time t, q_e is the maximum adsorption capacity (mg/g), k is the rate constant (min), and n is the reaction order.

The formula of the pseudo-second-order value is shown below:

$$\frac{1}{q_t} = \left(\frac{1}{k_2 {q_e}^2}\right)\left(\frac{1}{t}\right) + \frac{1}{q_e}$$

where, q_t is the amount of dye adsorbed (mg/g) at time *t*, q_e is the maximum adsorption capacity (mg/g), k_2 is the second-order rate constant (min).

Using a UV-vis spectrophotometer, the total sorption capacity is measured at different initial dye concentrations, and the maximum sorption capacity values are represented as adsorbed dye concentration (mg/g) vs. different initial dye concentrations.

During this analysis, isothermal models for Langmuir, Freundlich, and BET adsorption were used [55,56]. The isotherm of Langmuir is widely used for describing single-solute systems [57]. The following formula is given to the Langmuir isotherm:

$$q_e = \frac{q_m C_e K_L}{1 + C_e K_L} \quad =====> \quad \frac{1}{q_e} = \frac{1}{q_m} + \left(\frac{1}{q_m K_L}\right)\left(\frac{1}{C_e}\right)$$

where q_e is the concentration at dye equilibrium on the membrane (mg/g), q_m is the concentration of equilibrium dye in solution (mg/l), q_m is the maximum capacity of the membrane (mg/g), and K_L is the constant of Langmuir (L/mg) adsorption. The linearization of the $1/q_e$ versus $1/C_e$ Langmuir isotherm plotting gives a straight line with a $1/q_eK_L$ slope and a $1/q_m$ intercept.

For describing heterogeneous structures, the Freundlich isotherm is fine. [57] The isothermal formula of Freundlich is as follows:

$q_e = q_e C_e^{1/n}$=====> $ln(q_e) = ln(K_F) + \frac{1}{n} ln(C_e)$

where q_e is the concentration of equilibrium dye on the membrane surface (mg/g), C_e is the concentration of equilibrium dye in solution (mg/l), K_F is the Freundlich adsorption constant (L/mg), and n is the heterogeneity variable.

3. Results and Discussion

3.1. Preparation of Cellulose Acetate

3.1.1. X-Ray Diffractometry (XRD)

Figure 1 showed XRD patterns of cotton extracted cellulose with H2SO4 in the hydrolysis process. The XRD hydrolyzed cotton pattern with sulphuric acid exhibits typical cellulose peaks of 2θ = 15 and 22°. The XRD of cellulose is the principal component of cotton. The crystallinity of cellulose was achieved at 15.38 and 21.86°C.

The most crystallinities of cellulose produced were subsequently processed to obtain cellulose acetate by acetylation. The cellulose and cellulose acetate XRD pattern comparison is shown in **Figure 1**. **Figure 1** demonstrates that the cellulose acetate XRD pattern doesn't differ much from the cotton extracted XRD cellulose pattern. XRD cellulose acetate pattern shows two peaks with 2 peaks at 15.70 and 22.44°, which are likewise typical cellulose peaks. The cellulose acetate peak intensity was nonetheless quite high. The addition of acetyl groups to the primary cellulose polymer chain was probably affected.

3.1.2. Fourier transform infrared spectroscopy (FT-IR)

The cellulose and cellulose acetate FT-IR spectra are illustrated in **Figure 2**. Cellulose absorption peaks derived from cotton have typical

cellulose absorption peaks. Absorption bands are attributable to OH vibration of wave number 3388.93 cm^{-1} [6-10]. A strong bond between H_2O and cellulose [2]. constitutes the absorption band at 1600 cm^{-1}. A wide OH vibration absorption band has been found after acetylation and moved to a lower wave number (3376.44 cm^{-1}). In the wave numbers 1737.86 and 2902.87 cm^{-1}, which matched the C = O and the CH vibrations respectively, the rise in intensities was also seen [11]. These findings have validated the cellulose acetylation procedure.

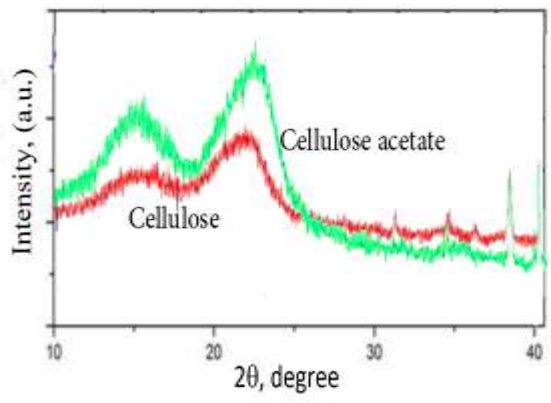

Figure 1: XRD pattern for cellulose and cellulose acetate

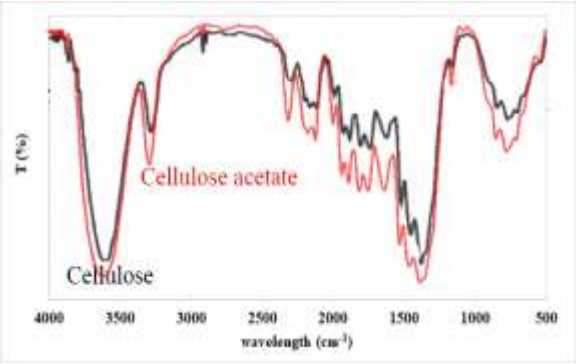

Figure 2: FT-IR spectra for cellulose and cellulose acetate

3.1.3. Scanning Electron Microscopy (SEM)

SEM has been used to examine the morphology of cellulose and cellulose acetate as shown in **Figure 3**. The SEM image of cellulose extracted from cotton shows an elongated threadlike structure which was the initial structure of the cotton. The structure of cotton was almost retained after hydrolysis (cellulose) but it only physically changed after acetylation processes (cellulose acetate). This result also agreed with the XRD analysis, where the XRD pattern of cellulose and cellulose acetate was not significantly different.

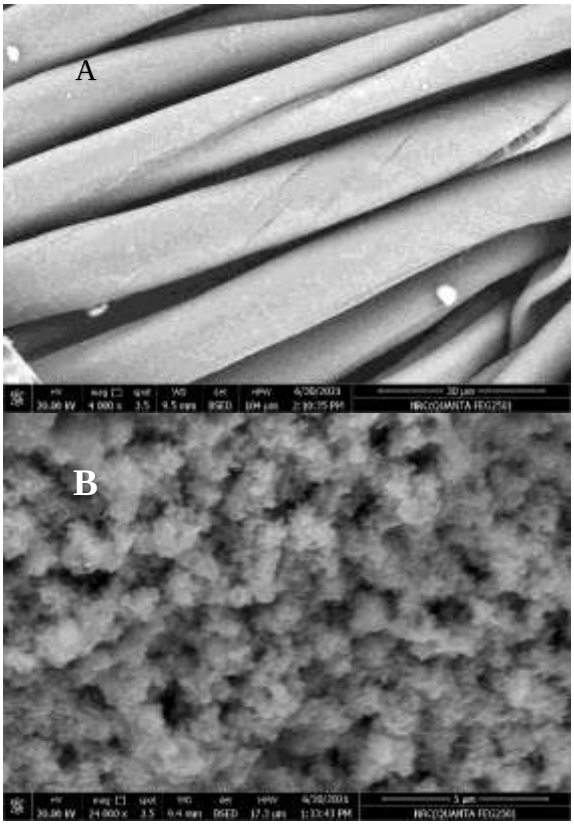

Figure 3: SEM image for synthesized Cellulose (A) and Cellulose acetate (B)

3.1.4. Modification and characterization of Cellulose acetate grafted POSS

3.1.4.1. The synthesis of CA–POSS additive

The POSS-modified cellulose acetate (CA–POSS) was synthesized via a two-step reaction as shown in **Figure 4**. The first step was the formation of isocyanate-functionalized POSS. The POSS nanoparticle used in this study was aminopropylisobutyl POSS. It has unreactive isopropyl groups on seven of the cage corners and a reactive aminopropyl group on the eighth corner. Since the reis one reactive functionality on the POSS compound, cross-linking is not possible and the POSS nanoparticles will exist as pendants on the CA chain. The toluene-2,4-diisocyanate (TDI) molecule has two isocyanate groups, each of which can react with a hydroxyl group. TDI is an asymmetric molecule and its two isocyanate groups have different reactivities. Due to steric hindrance within the molecule, the para-isocyanate reacts preferentially with the amine group of amino-propylisobutyl POSS [22]. In the second step, the ortho-isocyanate of TDI was reacted, using a tin catalyst, with the hydroxyl groups on the CA backbone to form CA–POSS. The ratios were selected such that each CA chain had approximately four pendant POSS groups on average.

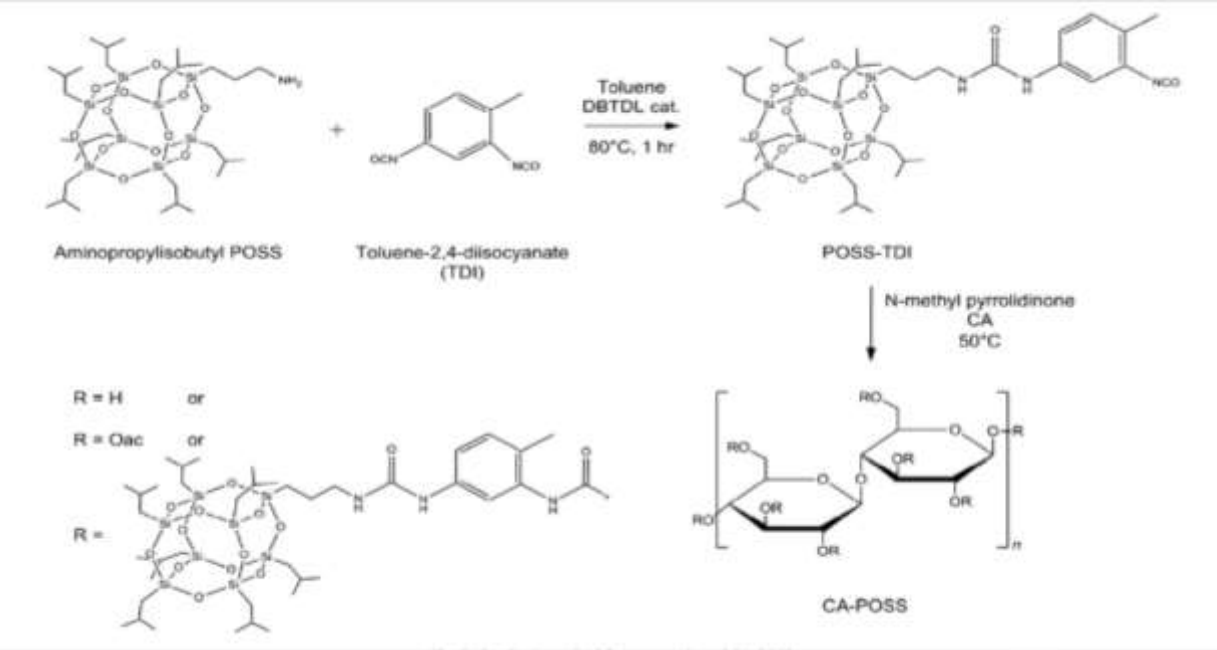

Figure 4: Synthesis of CA-POSS via a two-step reaction

3.1.4.2. CA–POSS characterization

The CA–POSS synthesis reaction was followed using ATR–FT-IR. **Figure 5** shows the spectra for POSS, POSS–TDI, CA–POSS, and CA. The ATR–FT-IR spectrum of CA displays characteristic cellulosic peaks at 3484 cm^{-1} (–OH stretching), 2944 and 2886 cm^{-1} (asymmetric and symmetric C–H stretching, respectively), 1730 cm^{-1} (C=O stretching), 1215 cm^{-1} (carboxylate C–O stretch), 1161 cm^{-1} (asymmetric stretching of the C–O–C bridge), and 1028 cm^{-1} (stretching of pyranose ring C–O–C). Characteristic peaks for aminopropylisobutyl POSS are observed at 2800–2950 cm^{-1} (C–H bond vibration), 1230 cm^{-1} (Si–C bonds), and 1072 cm^{-1} (Si–O–Si cage structure) [23,24]. In the spectrum of POSS–TDI, the appearance of a peak for the N–H bend at 1550 cm^{-1} from the urea linkage formed between POSS and TDI, and the characteristic band for the isocyanate group (N=C=O) observed at 2262 cm^{-1} indicate the completion of the POSS–TDI reaction [25,26]. After the reaction of the POSS– TDI with cellulose acetate, the spectrum of CA–POSS retains much of the character of cellulose acetate but notably has characteristic peaks at 2800–2950 and 1085 cm^{-1}, which are assigned for POSS. Also, the isocyanate peak from POSS–TDI (2262 cm^{-1}) is now absent, having been converted into a carbamate linkage (1650 cm^{-1}), thus confirming the covalent attachment of POSS to CA via TDI.

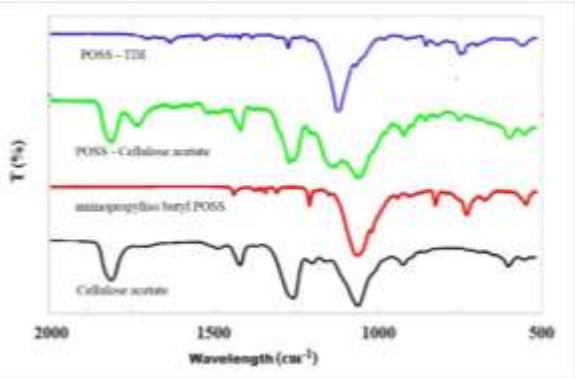

Figure 5: FT-IR spectra for cellulose acetate and its POSS modified

3.1.5. In-situ Preparation and characterization of different nano-metal and/or metal oxide in cellulose acetate/polymer composite

3.1.5.1. Characterization of Synthesized silver nanoparticles

The UV-Vis spectra of synthesized silver nanoparticles using modified cellulose acetate as a reducing and stabilizing agent were observed and illustrated in **Figure 6**. The UV-Vis spectrum of the colloidal solution of Silver Nanoparticles has a peak absorption of 460 nm, which is the characteristic peak for AgNPs. The color transition from the initial yellow to dark brown after 80°C in 10 minutes, suggests the development of silver nanoparticles (AgNPs). **[53]** Due to the polydisparities of

nanoparticles, the strong plasmon resonance at 417 nm was observed for synthesized AgNPs. **[54, 55]**

Figure 6 shows the TEM images of synthesized AgNPs using cellulose acetate. TEM images are shown as a spherical form of good distribution. The TEM study shows that the particles have small distribution ranges of 120 and 90 nm respectively.

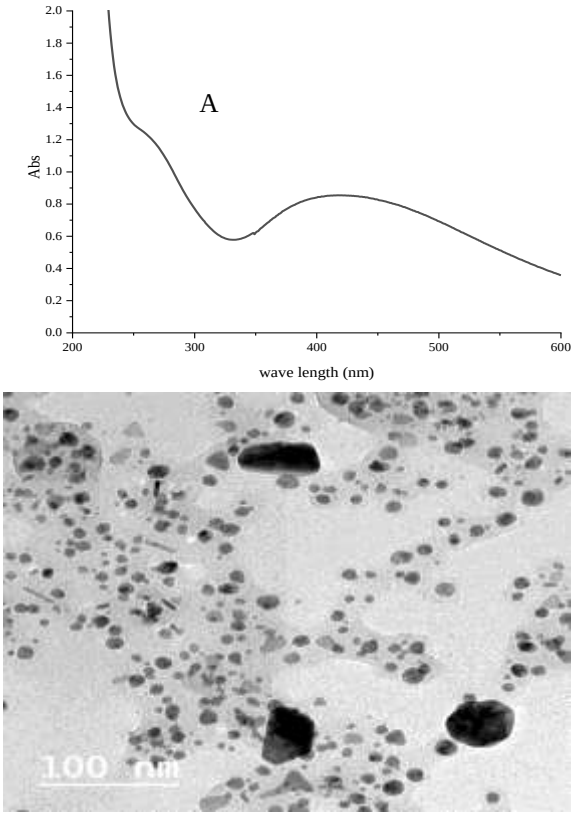

Figure 6: UV spectra, and TEM image for synthesized AgNPs
a) UV spectra of AgNPs, b) TEM image of synthesised AgNPs

Figure 7 shows the particle size of the synthesized AgNPs using modified cellulose acetate. This indicates that the size of AgNPs is around 100 nm due to the presence of cellulose acetate on the surface of AgNPs. On the other hand, **Figure 8** reveals that the negative signal value of zeta potential for AgNPs (-42.5 mV) is attributed to the surface charge of cellulose acetate and the effect of hydroxyl groups of its chain.

3.1.5.2. Characterization of synthesized ZnONPs

Figure 9 depicts that, the particle size of synthesized ZnONPs using modified cellulose acetate is ranged from about 137 nm. Coating of cellulose acetate onto the external surface of the ZnO nanoparticles could be proved from zeta potential measurements. **Figure 10** shows that the negative signal value of zeta potential for ZnONPs (-40.5 mV) is attributed to the surface charge of cellulose acetate and the effect of hydroxyl groups of its chain.

ZnONPs essentially consist of a 3D space that is periodically structured. X-rays must be dispersed by atoms of the sample. The dispersal of X-rays from arranged atoms creates diffractions in several directions which are common for these atoms. D-spacing values from the achieved peaks enable mineral identification since every element has a set of d-spacings that do not match. This is simply accomplished by contrasting d-spacings with regular reference patterns.

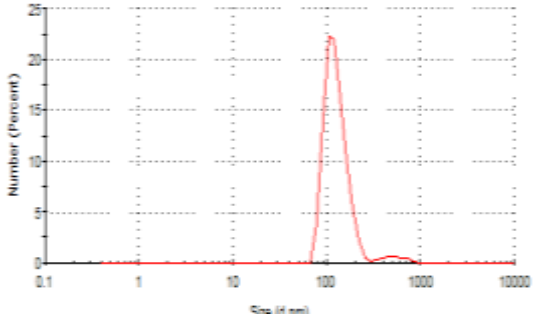

Figure 7: Particle size of synthesized AgNPs using cellulose acetate

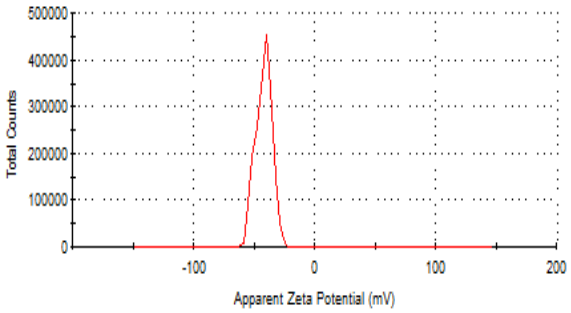

Figure 8: Zeta potential of synthesized AgNPs using cellulose acetate

The X-ray diagrams in **Figure 11** display the same high intensity and width sequence for all the examined synthesized ZnONPs. It reveals for synthesized ZnONPs that, the d-Spacing values at 2 Theta positions (2θ; 32.09, 34.81, 36.69, 47.87, and 56.99) for synthesized ZnONPs using cellulose acetate as a capping agent coincided with the results published by the many researchers in literature in terms of values 2.7, 2.5, 2.5, 1.8, and 1.6, respectively. **[22, 24, 29, 56]**

The coordinated ZnONPs have been studied for the decomposition of reduced zinc oxide with cellulose acetate by thermo-gravimetrical analyses (TGA).

Figure 12 indicates water loss accompanied by the decomposition of capping agents until approximately 290°C in the first stage of the thermal decomposition profile. However, the decomposition step ends around 320°C. In addition, this step provides that the weight loss percentage was around 58 %. Last phase stopping at 600°C offers ash loss of around 30% for final weight loss percent. In brief, a temperature of 0–400°C is enough to completely break down zinc compounds with a good weight loss ratio.

The TEM image of synthesized ZnONPs was shown in **Figure 14**. TEM image shows a good distribution spherical shape with small scatter sizes in nano form around 60 nm

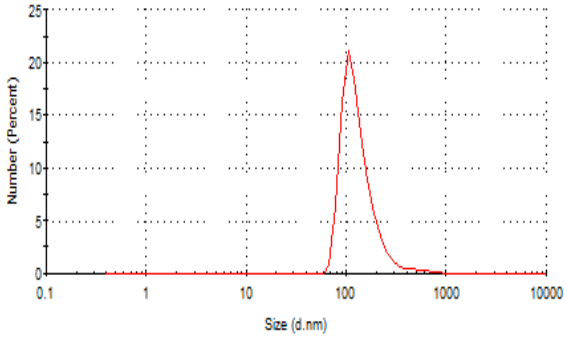

Figure 9: Particle size of synthesized ZnONPs using cellulose acetate

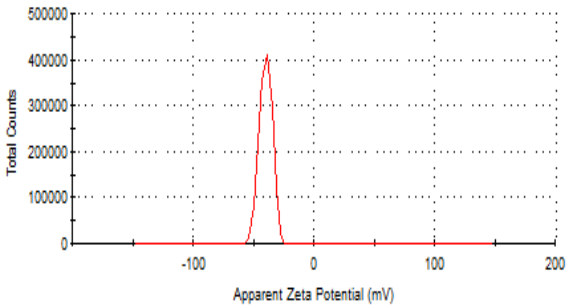

Figure 10: Zeta potential of synthesized ZnONPs using cellulose acetate

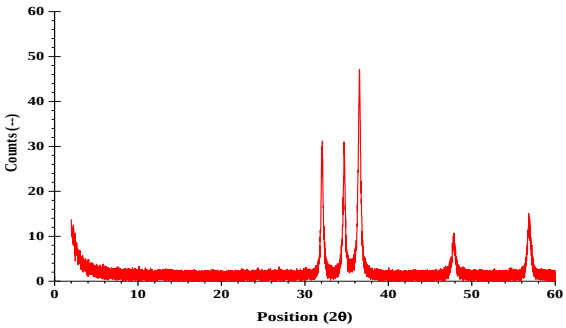

Figure 11: XRD for synthesized ZnONPs

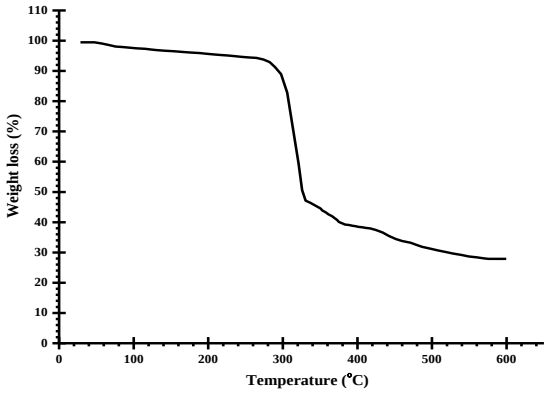

Figure 12: TGA for synthesized ZnONPs

3.1.5.3. Characterization of synthesized ZrO2NPs

The XRD patterns of the ZrO_2 were calcined at 600°C for 5 hours and are shown in Figure 13. Pure ZrO_2 shows both monoclinic (2θ = 27 and 31.1°) and tetragonal (2θ = 30, 34.9, 50 and 60°) phase. Scherer equation was used to calculate the crystallite sizes for the ZrO_2 it was estimated to be 18.1 nm. It should be noted that cellulose acetate has a significant effect on the resulting ZrO_2 crystallite size.

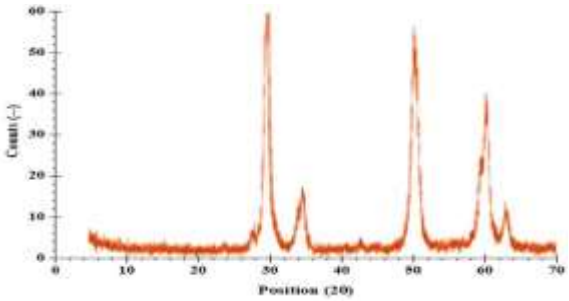

Figure 13: XRD pattern for synthesized ZrO2NPs

The particle composition was also studied by TEM and SEM and the images are shown in **Figure 14** and **Figure 15**. **Figure 14** shows the TEM image of zirconia nanoparticles synthesized by the sol-gel method using zirconium isopropoxide, The estimated diameters of nanoparticles were found to be around 25 nm. It could be seen that the particles are uniform and spherical and the average particle size calculated was about 10 nm. There is a slight difference in the size of particles obtained from TEM compared to the crystallite size obtained by XRD. This can be attributed to differences in the accuracy of measurements of the two different techniques

Figure 15, shows the SEM image of ZrO_2 obtained from zirconium isopropoxide precursor and cellulose acetate. it appears to have a defined shape.

The image appears to show particles like a broken rib cage. Due to this ill-defined morphology, it is possible that the SEM does not give a clear idea of the formation of nanoparticles in this case.

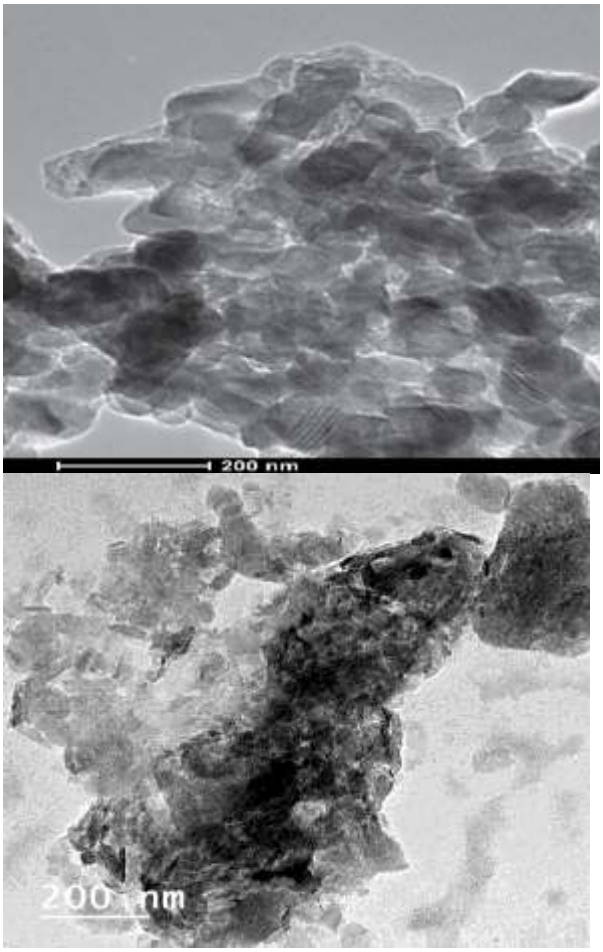

Figure 14: **TEM image for synthesized ZrO_2NPs**

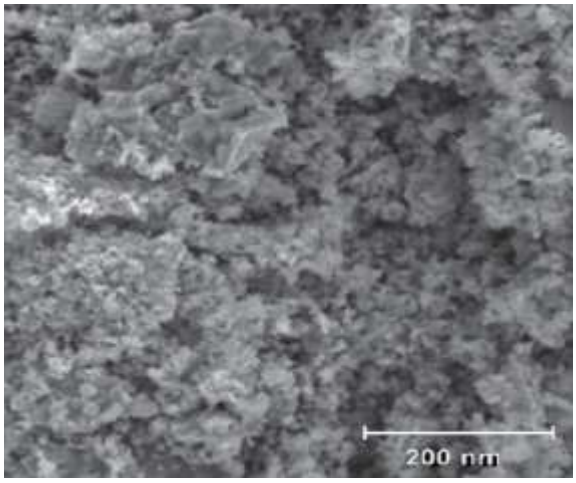

Figure 15: **SEM image for synthesized ZrO_2NPs**

3.1.5.4. Characterization of synthesized SiO2NPs

XRD of SiO_2 nanoparticles as shown in **Figure 16**. As for the XRD patterns of pure SiO_2, a characteristic peak at 24° due to the noncrystalline diffraction from amorphous silica is observed [57].

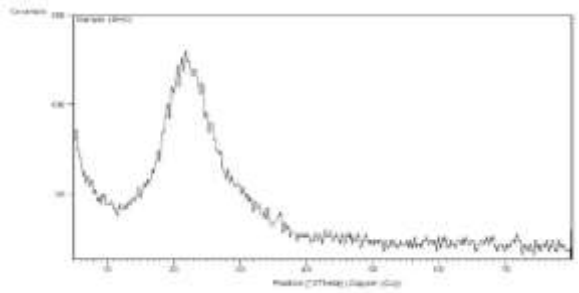

Figure 16: XRD of SiO_2 nanoparticles

Figure 17 shows TEM images of the synthesized samples with various magnifications. These images indicate the structure of colloidal particles may be spherical or slightly irregular in shape, and they seem to be present as slightly structured aggregates. Furthermore, particle size data represented in **Figure 18** depicts that, silica nanoparticles have been successfully prepared. The sizes of the silica nanoparticles have a maximal are a range of around 120 nm.

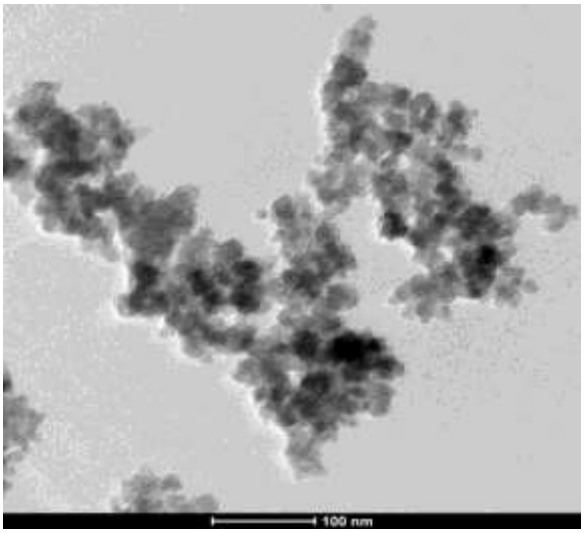

Figure 17: TEM images of synthesized SiO_2 colloidal

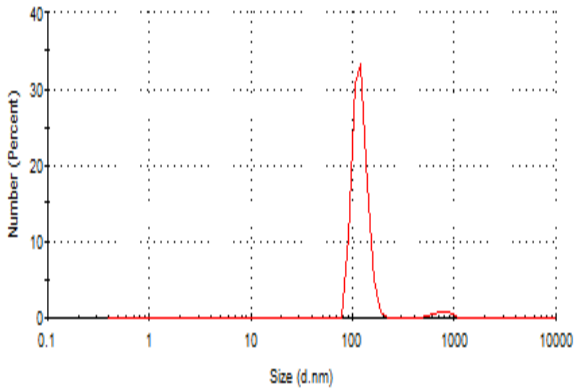

Figure 18: Particle size of silica nanoparticles

The stability of the as-prepared silica colloidal solution depends on the density of charges that existed upon its surface. By measuring Zeta potential (**Figure 19**), it would be able to demonstrate the stability of silica colloidal solution. Zeta potential values near zero indicate that the particles in the mixture are likely to stick together when they collide unless they also are stabilized by non-electrical factors. [58]**.**

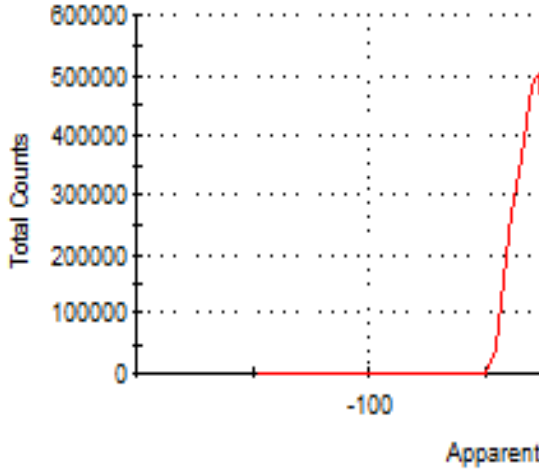

Figure 19: Zeta potential of silica nanoparticles

3.1.5.5. Characterization of synthesized TiO2NPs

To determine the crystal structure, we performed XRD studies on TiO_2NPs as shown in **Figure 20**. TiO_2NPs exhibited multiple diffraction peaks, which can be indexed to the anatase phase (JCPDS File No. 21- 1272) of TiO_2. In addition, the crystallite type of the TiO_2NPs was pure anatase. These data are in agreement with that of Balachandaran et al. [59]. The results confirmed the transformation of the amorphous to anatase phase of the TiO_2 shell.

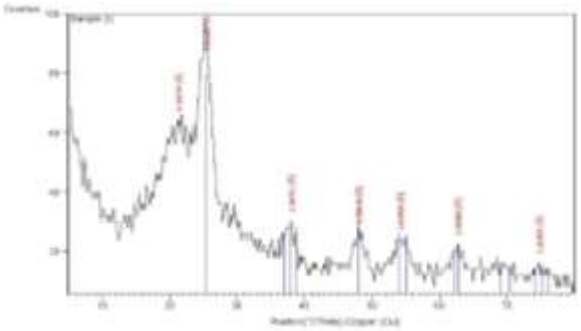

Figure 20: XRD of TiO_2NPs

Typical SEM and TEM images of the prepared TiO_2NPs are presented in **Figure 21**. It was obvious from the TEM images that the as-prepared TiO_2NPs have a definite shape with the smallest size.

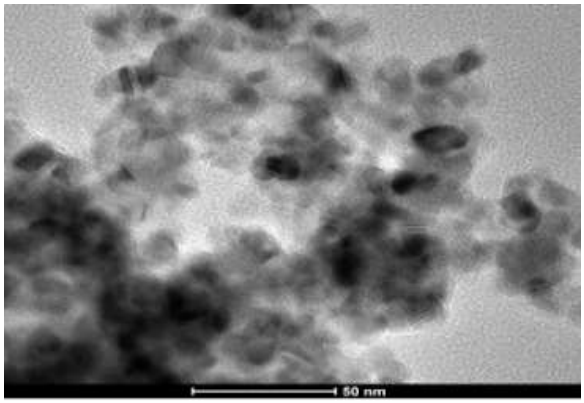

Figure 21: TEM image of TiO_2NPs

Figure 22 provides the particle size and size distribution of **TiO_2NPs**. The nanoparticles have a smaller particle size. It was understandable that the nano-particulate systems having smaller PDI are the more homogeneous.

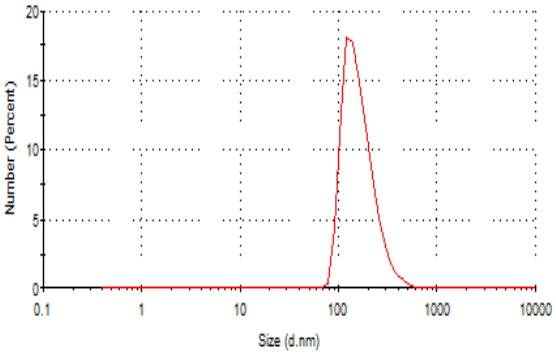

Figure 22: Particle size of TiO_2NPs

The zeta potential (surface charge) measurements are a measure of the electric charge at

the surface of nanospheres, being an indirect measure of their physical stability. **Figure 23** shows the Zeta potential of prepared TiO_2NPs.

It is seen that the Zeta potential value equals -31.1 mv. The obtained negative values for Zeta potential for TiO_2NPs can be explained by a negatively charged surface, which is created by the great number of hydroxyl groups available in cellulose acetate molecules.

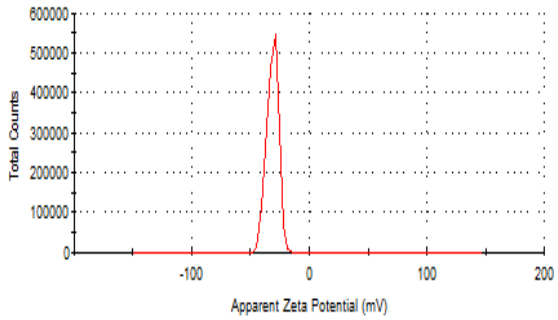

Figure 23: Zeta potential of TiO_2NPs

3.1.6. Characterization of cellulose acetate membrane

3.1.6.1. Morphological behavior

Modified cellulose acetate membrane with different nanoparticles has been investigated, using a scanning electron microscope and it is shown in **Figure 24**, which provides homogenesis distribution of nanometals across the modified cellulose acetate membrane

3.1.6.2. Determination of Surface Area and Pore Diameter

Nitrogen adsorption-desorption isotherms at liquid nitrogen temperatures were obtained for modified cellulose acetate membrane (MCM) obtained with and without metal nanoparticles by in-situ and ex-situ methods. One of the important properties is the special surface area for the modified cellulose acetate membrane (MCM) with and without metal nanoparticles. **Table 1** provides the specific area and diameter of the surface for different membranes. The results presented in **Table 1** show that the MCM membrane has a smaller specific surface area with 105.24 m^2/g than another membrane with different metal nanoparticles. Such effects can be due to the small particle diameter and drying efficiency.

3.1.6.3. Color removal studies

The effect of composition and amount of modified cellulose acetate membrane (MCM) (0.5-20 g/l) on RB5 (100 mg/L) color removal was studied.

The percentage of color removal of RB5 versus the number of different membranes is shown in **Table 2** and

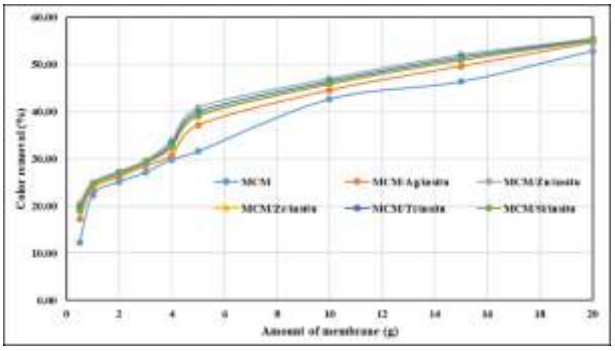

Figure 25. The results showed that the color removal % of RB5 was linearly proportional to the amount of membrane.

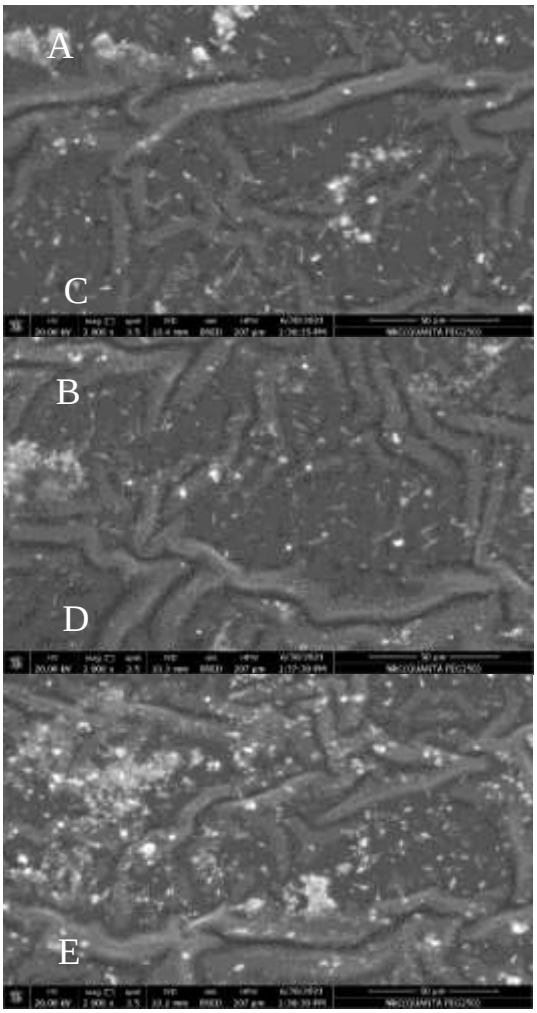

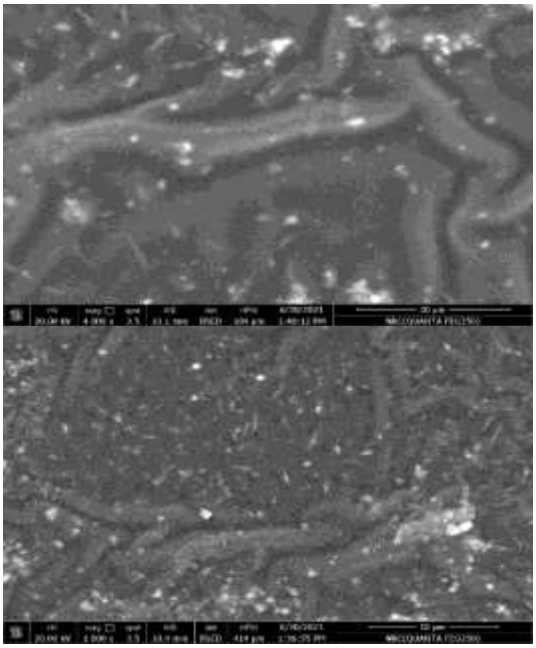

Figure 24: SEM image for Prepared cellulose acetate membrane in presence of different nanoparticles (a) AgNPs, (b) ZnONPs, (c) TiO_2NPs, (d) ZrO2NPs and (e) SiO2NPs

Table 1: Physical properties for prepared membrane with and without metal nanoparticles (in-situ and ex-situ)

Membrane	BET Surface Area (m^2/g)	Total pore volume (m^3/g)	Mean pore diameter (nm)
MCM	105.24	0.34	44.80
MCM/Ag/in-situ	325.48	0.78	24.33
MCM/Zn/in-situ	333.62	0.80	24.94
MCM/Zr/in-situ	341.96	0.82	25.57
MCM/Ti/in-situ	350.50	0.84	26.20
MCM/Si/in-situ	359.27	0.86	26.86
MCM/Ag/ex-situ	220.05	0.46	31.10
MCM/Zn/ex-situ	225.55	0.47	31.88
MCM/Zr/ex-situ	231.19	0.48	32.67
MCM/Ti/ex-situ	236.97	0.50	33.49
MCM/Si/ex-situ	242.89	0.51	34.33

During the in-situ method, preparation of membrane, a large excess of modified cellulose acetate would be completely covered the surface of nanoparticles. Assuming that the active sites for the electrostatic attraction with RB5 are high, therefore, the color removal reaction on the surface of the prepared membrane will be faster at a low amount of adsorbent.

By means, fewer amounts of metal nanoparticles are effectively bound on the surface of the membrane at an initial concentration of < 4 g/l. Based on the dosage of the membrane. The improvement in color removal (percentage) with increased dosage of the membrane was attributed to the availability at a higher dose of more surface-efficient types.

The further increase in membrane concentration above 10 g/l has no major (percent) effect on color removal. It has not negatively impacted the peak adsorption efficiency at 10 g/l. This can be related to the equilibrium reached when membrane potential is stabilized or at a higher concentration due to the self-crosslinking of metal nanoparticles.

3.1.7. Adsorption study

3.1.7.1. Kinetic study

Adsorption efficiency and test feasibility are provided using helpful information from processes of kinetic adsorption.

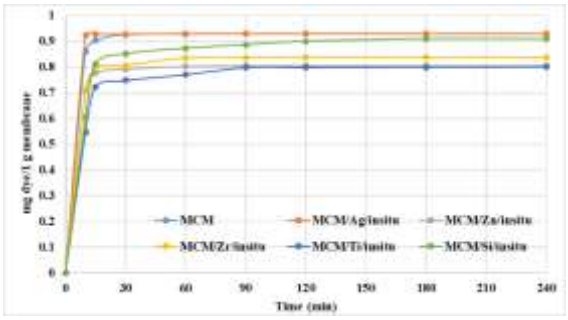

Figure 26 shows the concentration-time curves of RB5 adsorption on the prepared membranes, with each process having a different membrane concentration. It's obvious from the chart that prepared composite with both methods (in-situ or ex-situ) and initial dye concentrations from 100 mg/100 ml can adsorb RB5 with good exhausting from the dye bath solution. In addition, using a membrane with metal nanoparticles by in-situ method shows better absorption behavior than using a membrane with metal nanoparticles by ex-situ method, especially at the first 20 mins which confirms that the prepared membranes through the in-situ method have small cavities which have the opportunity to absorb the dye molecules and keep it inside its network more than the prepared membrane through ex-situ method.

In addition, in the membrane prepared through the in-situ method absorb dye molecules reach the maximum capacity after about 20 min, and further time shows a slightly increasing in dye absorption. But, in the case of prepared composite through deposition method, absorption of dye molecules reaches the maximum capacity after about 30 min

and further time shows a slightly increasing in dye absorption.

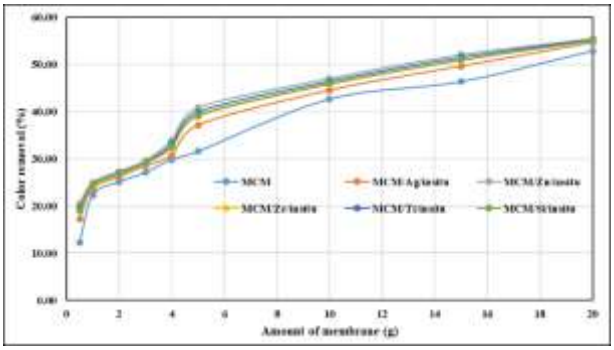

Figure 25: Color removal % of RB5 using a prepared membrane with and without metal nanoparticles (in-situ)

Table 2: Color removal % of RB5 using prepared membrane with and without metal nanoparticles (in-situ and ex-situ)

	Color removal (%)					
membrane weight (g)	MCM	MCM/Ag/in-situ	MCM/Zn/in-situ	MCM/Zr/in-situ	MCM/Ti/in-situ	MCM/Si/in-situ
0.5	12.21	17.26	20.49	18.88	19.68	19.08
1	22.31	23.73	24.93	24.33	24.63	24.40
2	25.14	26.13	27.31	26.72	27.01	26.79
3	27.11	28.49	29.61	29.05	29.33	29.12
4	29.87	30.73	33.93	32.33	33.13	32.53
5	31.59	37.12	40.81	38.97	39.89	39.20
10	42.65	44.50	47.05	45.78	46.41	45.93
15	46.35	49.60	52.11	50.85	51.48	51.01
20	52.85	54.61	55.49	55.05	55.27	55.11

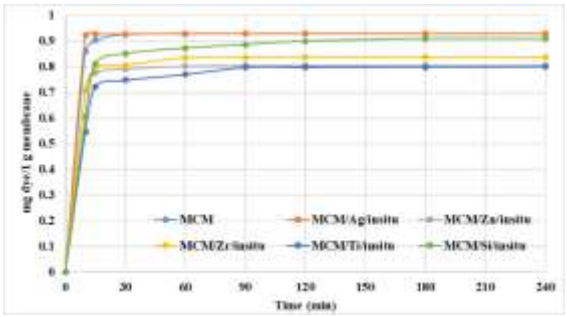

Figure 26: Contact time curves for RB5 with different membranes

The values of the adsorption rate constant (k), other parameters, and the correlation coefficient for RB5 adsorption on the membrane with different nano metals by both methods were determined for each plot from the kinetic adsorption processes.

Attaining the maximum linear relationship (the highest value of R^2) is the value for the reaction's chosen order. **Table 3** and **Table 4** display the respective values of rate constant (k) and R^2 correlation coefficients. C_{max} rose in the same direction as the data presented in

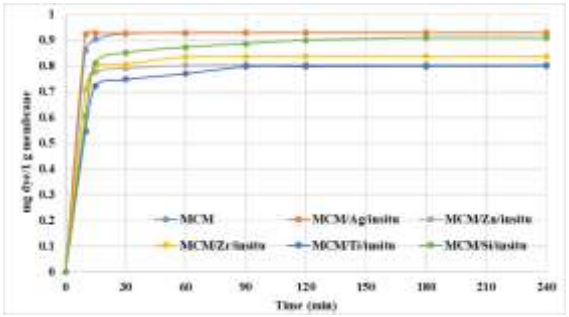

Figure 26 as the data presented in **Table 3** and **Table 4**. In short, as the concentration of processed material decreased from 2.5 to 30 mg/100 ml, the measured total dye efficiency (C_{max}) consumed from the examined models was increased for pseudo-first and pseudo-second-order.

From

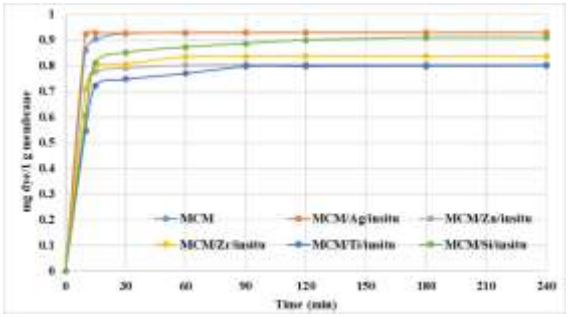

Figure 26, these data are collected and tested. Both values are nearest to one from the correlation coefficient (R^2) values. However, it is much closer to one with pseudo-second-order, so both techniques used (in-situ and ex--situ) obey pseudo-second-order with all concentrations. The second-order kinetic model suggests that the adsorption process by mean micro-pores is a diffusional one.

3.1.7.2. Isothermal studies

Adsorbed dye concentration (mg/g) vs. different initial dye concentrations shown in

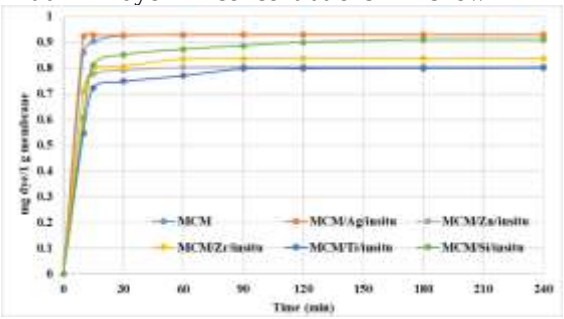

Figure 26 shows that by increasing the membrane concentration in the dye bath from 2.5 to 30 g/100 ml, the total adsorbed dye concentration has been improved. Langmuir and Freundlich's designs are the most widely used models. **Table 5** and **Table 6** list the isothermal system parameters with their regular errors. The Langmuir isotherm is commonly used to analyze single-solute structures and their prediction that intermolecular forces will decrease rapidly with separation and thus envisage monolayer dye coat on the prepared membrane outer surface. The facilitating presumption is that adsorption occurs at different homogeneous sites of the aerogel surface generated. There is no broad interaction between adsorbed species. Freundlich isotherm helps characterize heterogeneity and has been used to analyze RB5 adsorption on the membrane layer. As it can see, the Langmuir adsorption model shows stronger R^2 results than the other versions did. However, the fit to the Langmuir template indicates that RB5 dye can adsorb and form a monolayer on the active membrane sites. It defined a positive adsorption state from Freundlich's template as n value > 1, in this manner [72,73].

Table 3: Kinetic parameter values from the experimental data for pseudo-first-order parameters

Membrane	Pseudo-first-order parameters		
	qmax (mg/g)	K1 (min-1)	R2
MCM	91.24047619	0.0165	0.88505
MCM/Ag/in-situ	140.6	0.0196	0.8397
MCM/Zn/in-situ	121.8	0.02265	0.8622
MCM/Zr/in-situ	181.2	0.02135	0.8682
MCM/Ti/in-situ	104.0555556	0.0207	0.7662
MCM/Si/in-situ	180	0.02815	0.9011
MCM/Ag/ex-situ	41.88095238	0.0134	0.9304
MCM/Zn/ex-situ	122.2682927	0.0233	0.7054
MCM/Zr/ex-situ	80.61904762	0.0175	0.883
MCM/Ti/ex-situ	56.625	0.02055	0.797
MCM/Si/ex-situ	117.9565217	0.031	0.9086

Table 4: Kinetic parameter values from the experimental data for pseudo-second-order parameters

Membrane	Pseudo-second-order parameters		
	qmax (Exp.) (mg/g)	K1 (min-1)	R2
MCM	87.35746951	3.73359E-05	0.9969
MCM/Ag/in-situ	131.8125	3.07693E-05	0.9953
MCM/Zn/in-situ	107.9375	0.0000375	0.9951
MCM/Zr/in-situ	169.875	2.64706E-05	0.9955
MCM/Ti/in-situ	110.1764706	0.00015625	0.9996
MCM/Si/in-situ	190	1.95652E-05	0.9891
MCM/Ag/ex-situ	42.90243902	4.39025E-05	0.9985
MCM/Zn/ex-situ	125.325	6.66665E-05	0.9988
MCM/Zr/ex-situ	82.58536585	0.000045	0.9992
MCM/Ti/ex-situ	59.08695652	0.000204167	0.9997
MCM/Si/ex-situ	127.8636364	2.22222E-05	0.9955

Table 5: Parameters of Langmuir adsorption isotherm.

Membrane	Langmuir adsorption isotherm parameter			
	qmax (mg/g)	kL	RL	R2
MCM	81.34920635	0.000010768	0.394642317	0.99665
MCM/Ag/in-situ	83.33333333	0.000012896	0.378100424	0.9992
MCM/Zn/in-situ	74.07407407	0.000029268	0.288733615	0.9999
MCM/Zr/in-situ	83.33333333	0.000019456	0.336383208	0.9997
MCM/Ti/in-situ	92.59259261	0.000018876	0.339696991	0.9748
MCM/Si/in-situ	87.71929826	0.000027048	0.29829376	0.9884
MCM/Ag/ex-situ	79.36507936	0.00000864	0.411184211	0.9941
MCM/Zn/ex-situ	81.300813	0.000014568	0.366515174	0.9966
MCM/Zr/ex-situ	79.36507936	0.000011604	0.387566856	0.9955
MCM/Ti/ex-situ	69.44444446	0.000015924	0.35762821	0.9975
MCM/Si/ex-situ	72.46376813	0.000028584	0.291613204	0.9987

Table 6: Parameters of Freundlich adsorption isotherm.

Membrane	Langmuir adsorption isotherm parameter		
	KF	1/n	R2
MCM	2.364361709	0.12734	0.986
MCM/Ag/in-situ	4.399319188	0.0944	0.9764
MCM/Zn/in-situ	1.431824933	0.12576	0.9921
MCM/Zr/in-situ	2.2980244	0.113	0.9872
MCM/Ti/in-situ	0.903327778	0.14418	0.9844
MCM/Si/in-situ	0.526373684	0.15254	0.9925
MCM/Ag/ex-situ	0.32940423	0.16028	0.9956
MCM/Zn/ex-situ	0.16281	0.17262	0.9983
MCM/Zr/ex-situ	0.216607143	0.16776	0.9974
MCM/Ti/ex-situ	0.931504167	0.13574	0.9908
MCM/Si/ex-situ	0.389109565	0.15648	0.9962

4. Conclusion

Cellulose acetate was successfully prepared from cotton waste. The produced cellulose derivative was modified to introduce silicon moieties to its chemical structure. The modified material was used for in situ preparation of some nanoparticles such as silver, zinc, zirconium, titanium, and silica. The prepared nanoparticles were characterized using TEM, SEM, and XRD. The characterizations show that all the nanoparticles were successfully prepared with good morphological properties.

5. Conflict of interest

We confirm that there is no conflict of interest.

6. Acknowledgment

The authors gratefully acknowledge the National Research Centre (NRC) for providing the financial support for the in-house project No. 120306, and for the assistance of the laboratories in the Textile Research and Technology Institute, Scientific Centre of Excellence Laboratories Network, Sol-gel Lab, and the Electric and Dielectric Measurement Unit in conducting the necessary analyses for this study. In addition to Misr Spinning and Weaving Company, Al-Mahalla Al-Kubra and CSA Textile Egypt S.A.E Company for providing the necessary materials for this study.

7. References

[1]. M.T. Amin, A.A. Alazba, A review of nanomaterials based membranes for removal of contaminants from polluted waters, Membrane Water Treatment 5(2) (2014) 123-146.

[2]. N. Li, R. Bai, Copper adsorption on chitosan–cellulose hy¬drogel beads: Behaviors and mechanisms, Separation Purification Technology 42 (2005) 237-284.

[3]. E.N. Kallman, V.A. Oyanedel-Craver, J.A. Smith, Ceramic filters impregnated with silver nanoparticles for point-of-use water treatment in rural guatemala, Journal of Environmental Engineering 137(6) (2011) 407-415.

[4]. M.A. Eltawil, Z. Zhengming, L. Yuan, A review of renewable energy technologies integrated with desalination systems, Renewable and Sustainable Energy Reviews 13(9) (2009) 2245-2262.

[5]. G.R. Guillen, Preparation and characterization of membranes formed by nonsolvent induced phase separation: A review, Indust. Eng. Chem. Res. 50(7) (2011).

[6]. J.V. Rie, W. Thielemans, Cellulose–gold nanoparticle hybrid materials, Nanoscale Research Letters 9 (2017) 8525.

[7]. J. Pang, X. Liu, X. Zhang, Y. Wu, R. Sun, Fabrication of cellulose film with enhanced mechanical properties in ionic liquid 1-allyl-3-methylimidaxolium chloride (amimcl), Materials (Basel) 6(4) (2013) 1270-1284.

[8]. E. Blanchi, E. Marsano, L. Ricco, G. Conio, Derivatization of cellulose in homogeneous condition: 1-cellulose propionate, Carbohydrate Polymers 34(1) (1997) 91-94.

[9]. C.A. Cateto, A. Ragauskas, Amino acid modified cellulose whiskers, RSC Adv. 1(9) (2011) 1695-1697.
[10]. X. Zhang, M. Chen, C. Liu, A. Zhang, R. Sun, Ring-opening graft polymerization of propylene carbonate onto xylan in an ionic liquid, Molecules (Basel, Switzerland) 20(4) (2015) 6033-6047.
[11]. L.Y. Ng, A.W. Mohammad, C.P. Leo, N. Hilal, Polymeric membranes incorporated with metal/metal oxide nanoparticles. A comprehensive review, Desalination 308 (2013) 15–33.
[12]. H. Rabiee, V. Vatanpour, M.H.D.A. Farahani, H. Zarrabi, Improvement in flux and antifouling properties of pvc ultrafiltration membranes by incorporation of zinc oxide (zno) nanoparticles, Separation and Purification Technology 156 (2015) 299–310.
[13]. S. Anitha, B. Brabu, J.T. D., C. Gopalakrishnan, T.S. Natarajan, Optical, bactericidal and water repellent properties of electrospun nano-composite membranes of cellulose acetate and zno, Carbohydrate Polymers 87 (2012) 1065.
[14]. A.G. Hassabo, A.L. Mohamed, A.A. Nada, N.Y.A. Zeid, Controlled release of drugs from cellulosic wound bandage using silica microsphere as drug encapsulator module, JAPS 5(12) (2015) 067-073.
[15]. A.G. Hassabo, A.A. Nada, H.M. Ibrahim, N.Y. Abou-Zeid, Impregnation of silver nanoparticles into polysaccharide substrates and their properties, Carbohydrate Polymers 122 (2015) 343-350.
[16]. A.A. Nada, A.G. Hassabo, H.M. Awad, W. Fayad, N.M. Shaffie, A.A. Sleem, N.Y.A. Zeid, Biomaterials based on essential fatty acids and carbohydrates for chronic wounds, JAPS 5(10 (Suppl 3)) (2015) 13-21.
[17]. N.S. Elshemy, A.G. Hassabo, Z.M. Mahmoud, K. Haggag, Novel synthesis of nano-emulsion butyl methacrylate/acrylic acid via micro-emulsion polymerization and ultrasonic waves, JTATM 10(1) (2016) 1-16.
[18]. A.G. Hassabo, A.L. Mohamed, Multiamine modified chitosan for removal metal ions from their aqueous solution BioTechnology: An Indian Journal 12(2) (2016) 59-69.
[19]. A. Hebeish, S. Shaarawy, A.G. Hassabo, A. El-Shafei, Eco-friendly multifinishing of cotton through inclusion of motmorillonite/chitosan hybrid nanocomposite, Der Phar. Chem. 8(20) (2016) 259-271.
[20]. A.L. Mohamed, M.E. El-Naggar, T.I. Shaheen, A.G. Hassabo, Novel nano polymeric system containing biosynthesized core shell silver/silica nanoparticles for functionalization of cellulosic based material, Microsys. Technol. 22(5) (2016) 979-992.
[21]. A.A. Nada, A.G. Hassabo, A.L. Mohamed, M.M. Mounier, N.Y. Abou Zeid, Liposomal microencapsulation of rodent-repelling agents onto jute burlaps: Assessment of cytotoxicity and rat behavioral test, JAPS 6(8) (2016) 142-150.
[22]. M.E. El-Naggar, A.G. Hassabo, A.L. Mohamed, T.I. Shaheen, Surface modification of sio2 coated zno nanoparticles for multifunctional cotton fabrics, J. Colloid Interface Sci. 498 (2017) 413-422.
[23]. A.G. Hassabo, A.L. Mohamed, Enhancement the thermo-regulating property of cellulosic fabric using encapsulated paraffins in modified pectin, Carbohydrate Polymers 165 (2017) 421-428.
[24]. N.A. Ibrahim, A.A. Nada, A.G. Hassabo, B.M. Eid, A.M. Noor El-Deen, N.Y. Abou-Zeid, Effect of different capping agents on physicochemical and antimicrobial properties of zno nanoparticles, Chem. Pap. 71(7) (2017) 1365-1375.
[25]. A.L. Mohamed, M.E. El-Naggar, T.I. Shaheen, A.G. Hassabo, Laminating of chemically modified silan based nanosols for advanced functionalization of cotton textiles, Int. J. Biol. Macromol. 95 (2017) 429–437.
[26]. A.L. Mohamed, A.G. Hassabo, A.A. Nada, N.Y. Abou-Zeid, Properties of cellulosic fabrics treated by water-repellent emulsions, Indian J. Fibre Text. Res. 42(June) (2017) 223-229.
[27]. A.L. Mohamed, A.G. Hassabo, S. Shaarawy, A. Hebeish, Benign development of cotton with antibacterial activity and metal sorpability through introduction amino triazole moieties and agnps in cotton structure pre-treated with periodate, Carbohydrate Polymers 178 (2017) 251-259.
[28]. A.G. Hassabo, A.L. Mohamed, S. Shaarawy, A. Hebeish, Novel micro-composites based on phosphorylated biopolymer/polyethyleneimine/clay mixture for cotton multi-functionalities performance, Biosci. Res. 15(3) (2018) 2568-2582.
[29]. N.A. Ibrahim, A.A. Nada, B.M. Eid, M. Al-Moghazy, A.G. Hassabo, N.Y. Abou-Zeid, Nano-structured metal oxides: Synthesis, characterization and application for multifunctional cotton fabric, Adv. Nat. Sci.: Nanosci. Nanotechnol. 9(3) (2018) 035014.
[30]. A.G. Hassabo, M.E. El-Naggar, A.L. Mohamed, A.A. Hebeish, Development of multifunctional modified cotton fabric with tri-component nanoparticles of silver, copper and zinc oxide, Carbohydrate Polymers 210 (2019) 144-156.

[31]. A.G. Hassabo, A.L. Mohamed, Novel flame retardant and antibacterial agent containing mgo nps, phosphorus, nitrogen and silicon units for functionalise cotton fabrics, Biointerf. Res. Appl. Chem. 9(5) (2019) 4272 - 4278.
[32]. A.L. Mohamed, A.G. Hassabo, Review of silicon-based materials for cellulosic fabrics with functional applications, J. Text. Color. Polym. Sci. 16(2) (2019) 139-157.
[33]. A.G. Hassabo, S. Shaarawy, A.L. Mohamed, A. Hebiesh, Multifarious cellulosic through innovation of highly sustainable composites based on moringa and other natural precursors, Int. J. Biol. Macromol. 165 (2020) 141-155.
[34]. T.A. Khattab, A.L. Mohamed, A.G. Hassabo, Development of durable superhydrophobic cotton fabrics coated with silicone/stearic acid using different cross-linkers, Mater. Chem. Phys. 249(122981) (2020).
[35]. M.M. El-Zawahry, A.G. Hassabo, F. Abdelghaffar, R.A. Abdelghaffar, O.A. Hakeim, Preparation and use of aqueous solutions magnetic chitosan / nanocellulose aerogels for the sorption of reactive black 5, Biointerf. Res. Appl. Chem. 11(4) (2021) 12380 - 12402.
[36]. A.G. Hassabo, A.L. Mohamed, T.A. Khattab, Preparation of cellulose-based electrospun fluorescent nanofibers doped with perylene encapsulated in silica nanoparticles for potential flexible electronics, Luminescence n/a(n/a) (2021).
[37]. A.L. Mohamed, M.E. El-Naggar, A.G. Hassabo, Preparation of hybrid nano-particles to enhance the electrical conductivity and performance properties of cotton fabrics, Journal of Materials Research and Technology 12 (2021) 542-554.
[38]. A.L. Mohamed, A.G. Hassabo, Cellulosic fabric treated with hyperbranched polyethyleneimine derivatives for improving antibacterial, dyeing, ph and thermo-responsive performance, Int. J. Biol. Macromol. 170 (2021) 479-489.
[39]. M.Y. Yousef, A.G. Hassabo, Environmentally friendly inorganic materials for anti-flammable cotton fabrics, J. Text. Color. Polym. Sci. 18(2) (2021) 97-110.
[40]. M. Zayed, H. Othman, H. Ghazal, A.G. Hassabo, Psidium guajava leave extract as reducing agent for synthesis of zinc oxide nanoparticles and its application to impart multifunctional properties for cellulosic fabrics, Biointerf. Res. Appl. Chem. 11(5) (2021) 13535 - 13556.
[41]. A.L. Mohamed, A.G. Hassabo, Core–shell titanium@silica nanoparticles impregnating in poly (itaconic acid)/poly (n-isopropylacrylamide) microgel for multifunctional cellulosic fabrics, J. Polym. Res. 29(2) (2022) Article number: 68 (1-18).
[42]. A.L. Mohamed, S. Shaarawy, N. Elshemy, A. Hebeish, A.G. Hassabo, Treatment of cotton fabrics using polyamines for improved coloration with natural dyes extracted from plant and insect sources, Egy. J. Chem. (2022) -.
[43]. M. Zayed, H. Ghazal, H. Othman, A.G. Hassabo, Psidium guajava leave extract for improving ultraviolet protection and antibacterial properties of cellulosic fabrics, Biointerf. Res. Appl. Chem. 12(3) (2022) 3811 - 3835.
[44]. M. Zayed, H. Ghazal, H.A. Othman, A.G. Hassabo, Synthesis of different nanometals using citrus sinensis peel (orange peel) waste extraction for valuable functionalization of cotton fabric, Chem. Pap. 76(2) (2022) 639-660.
[45]. S. Al Aani, C.J. Wright, M.A. Atieh, N. Hilal, Engineering nanocomposite membranes: Addressing current challenges and future opportunities, Desalination 401 (2017) 1–15.
[46]. N.C. Mueller, B. van der Bruggen, V. Keuter, P. Luis, T. Melin, W. Pronk, R. Reisewitz, D. Rickerby, G.M. Rios, W. Wennekes, Nanofiltration and nanostructured membranes-should they be considered mnanotechnology or not?, J. Hazard. Mater. 211–212 (2012) 275–280.
[47]. A.F.T. Marino, M. Boerrigter, M. Faccini, C. Chaumette, L. Arockiasamy, J. Bundschuh, Photocatalytic activity and synthesis procedures of tio2 nanoparticles for potential applications in membranes, in: J.B.A. Figoli, J. Hoinkis, S.A. Altinkaya (Eds.), Application of nanotechnology in membranes for water treatment, CRC Press, Taylor & Francis Group: Abingdon, UK, 2017.
[48]. S.S. Madaeni, N. Ghaemi, H. Rajabi, Advances in polymeric membranes for water treatment, Elsevier Ltd, Amsterdam, The Netherlands, 2015.
[49]. M. Kabsch-korbutowicz, K. Majewska-nowak, T. Winnicki, Analysis of membrane fouling in the treatment of water solutions containing humic acids and mineral salts, Desalination 126 (1999) 179–185.
[50]. L. Yan, Y. Shui, C. Bao, Preparation of poly (vinylidene fluoride)(pvdf) ultrafiltration membrane modified by nano-sized alumina (al2o3) and its antifouling research, Polymer 46 (2005) 7701–7706.
[51]. E. Environ, M.M. Pendergast, E.M.V. Hoek, A review of water treatment membrane nanotechnologies, Energy Environ. Sci. 4 (2011) 1946–1971.
[52]. R. Rajendran, C. Balakumar, H.A.M. Ahammed, S. Jayakumar, K. Vaideki, E.M. Rajesh, Use of zinc oxide nano particles for production of antimicrobial textiles,

International Journal of Engineering, Science and Technology 2(2) (2010) 202-208.

[53]. E. Ajayi, A. Afolayan, Green synthesis, characterization and biological activities of silver nanoparticles from alkalinized cymbopogon citratus stapf, Adv. Nat. Sci.: Nanosci. Nanotechnol. 8(1) (2017) 015017.

[54]. R. Sathyavathi, M.B.M. Krishna, D.N. Rao, Biosynthesis of silver nanoparticles using moringa oleifera leaf extract and its application to optical limiting, Journal of Nanoscience and Nanotechnology 10 (2010) 1–5.

[55]. J.S. Moodley, S.B.N. Krishna, K. Pillay, Sershen, P. Govender, Green synthesis of silver nanoparticles from moringa oleifera leaf extracts and its antimicrobial potential, Adv. Nat. Sci.: Nanosci. Nanotechnol. 9(1) (2018).

[56]. A.L. Mohamed, A.G. Hassabo, Engineered carbohydrate based material/silane as a thermo and ph-sensitive nanogel containing zinc oxide nanoparticles for antibacterial textile, International Conference on Medical Textiles and Healthcare Products (MedTex 2015), Department of Material and Commodity Sciences and Textile Metrology, Faculty of Material Technologies and Textile Design, Lodz University of Technology, Lodz, Poland, 2015.

[57]. C.E. Thomas, A. Ehrhardt, M.A. Kay, Synthesis and characterizations of silica nanoparticles by a new sol-gel method, Nat Rev Genet 4 (2003) 346.

[58]. P. Tam, M. Monck, D. Lee, O. Ludkovski, E.C. Leng, K. Clow, H. Stark, P. Scherrer, R.W. Graham, P.R. Cullis, Surface modification of silica nanoparticles to reduce aggregation and nonspecific binding, Gene Ther. 7 (2000) 1867.

[59]. R. Venckatesh, K. Balachandaran, R. Sivaraj, Synthesis and characterization of nano tio2-sio2: Pva composite-a novel route, Int. Nano Lett. 2(1) (2012) 1-5.